atoms

MDPI

Article

Multi-Configuration Dirac–Hartree–Fock (MCDHF) Calculations for B-Like Ions

Indu Khatri [1,*], Arun Goyal [1], Avnindra Kumar Singh [2] and Man Mohan [1]

[1] Department of Physics and Astrophysics, University of Delhi, Delhi 110007, India; arun.goyal.du@gmail.com (A.G.); drmanmohan.05@gmail.com (M.M.)

[2] Department of Physics, D.D.U. College, University of Delhi, Delhi 110015, India; avni.physics@gmail.com

* Correspondence: indu.khatri.du@gmail.com

Academic Editor: James F. Babb

Received: 9 December 2015; Accepted: 5 April 2016; Published: 6 May 2016

Abstract: Relativistic configuration interaction results are presented for several B-like ions (Ge XXVIII, Rb XXXIII, Sr XXXIV, Ru XL, Sn XLVI, and Ba LII) using the multi-configuration Dirac–Hartree–Fock (MCDHF) method. The calculations are carried out in the active space approximation with the inclusion of the Breit interaction, the finite nuclear size effect, and quantum electrodynamic corrections. Results for fine structure energy levels for $1s^2 2s^2 2p$ and $2s2p^2$ configurations relative to the ground state are reported. The transition wavelengths, transition probabilities, line strengths, and absorption oscillator strengths for $2s^2 2p$–$2s2p^2$ electric dipole (E1) transitions are calculated. Both valence and core-valence correlation effects were accounted for through single-double multireference (SD-MR) expansions to increasing sets of active orbitals. Comparisons are made with the available data and good agreement is achieved. The values calculated using core–valence correlation are found to be very close to other theoretical and experimental values. The behavior of oscillator strengths as a function of nuclear charge is studied. We believe that our results can guide experimentalists in identifying the fine-structure levels in their future work.

Keywords: oscillator strength; radiative data; correlation; active set

1. Introduction

For ions with three electrons in the valence shell, it is quite simple to take all the configuration interactions between the states of the ground complex into consideration. Besides, three electron spectra are sufficiently complex to show unusual level anti-crossing effects. Due to increased availability of experimental data for highly-ionized systems obtained from beam-foil experiments and from astrophysical measurements, interest in transition rates and oscillator strengths in highly ionized atoms has increased. The calculated results are useful in the case of yet unobserved transitions and also for determining the density and temperature of the solar corona or in the diagnostic studies of thermonuclear plasmas. The X-ray spectra from L-shell ions lie in the wavelength region covered by the space observatories XMM-Newton and Chandra [1] and thus may be important for astrophysics. The spectral studies of boron-isoelectronic sequence are of great importance in diagnostics of solar, astrophysical, and fusion plasmas [2,3]. Transitions within $n = 2$ complex of ions in the boron isoelectronic sequences have been observed in tokamak [4,5] and astrophysical plasmas [6]. Transition within the $2s^2 2p$ ground configuration are particularly useful for diagnostics of electron densities in the range 10^{12} to 10^{14} cm^{-3} [7,8]. Germanium is a useful element for plasma diagnostics [9].

Theoretically, many authors have contributed to the study of boron-like ions [10–16]. Bhatia *et al.* [17] calculated oscillator strengths, radiative decay rates, and collision strengths for many ions including Ge XXVIII. Energy levels and rates for electric dipole transitions in boron like ions between B I and Si IX were presented by Fischer and Tachiev [18,19] using multi-configuration

Breit–Pauli wave functions. Fischer also calculated energy levels, transition rates, and lifetimes of boron-like ions using the multi-configuration Dirac–Hartree–Fock method [20]. Energy levels and transition rates were presented by Koc [21–23] based on the multireference relativistic configuration interaction method with the no-pair Dirac–Coulomb–Breit Hamiltonian. Corrégé and Hibbert [24] presented energy levels, oscillator strengths, and transition probabilities for C II, N III, and O IV using the CIV3 code. Energy levels, specific mass shift parameters, and transition probabilities for C II, N III, and O IV were presented by Jönsson *et al.* [25,26]. Hao and Jiang reported energy levels, transition rates, and line strengths for several ions along the B I isoelectronic sequence using multi-configuration Dirac–Hartree–Fock method [27]. Energies, transition rates, line strengths, oscillator strengths, and lifetimes were reported for boron-like ions between N III and Zn XXVI by Rynkun *et al.* [28]. Lifetime of the $2s^2 2p\ ^2P_{3/2}$ level and fine structure energy splitting between $^2P_{3/2}$ and $^2P_{1/2}$ levels in B-isoelectronic sequence were obtained by Marques *et al.* [29]. Energy, fine structure, hyperfine structure, and radiative transition rates of the high-lying multi-excited states for B-like Ne were obtained by Zhang *et al.* [30]. Chen [31] calculated energies, expectation values, fine structures, and hyperfine structures of the ground state and excited states for boron using the Rayleigh–Ritz variational method. An experimental study for transitions within $n = 2$ complex of Ba^{51+} has been made by Reader *et al.* [32].

In this paper, the MCDHF method is employed to determine fine structure energy levels, E1 wavelengths, transition probabilities, oscillator strengths, and line strengths between the states of $2s^2 2p$ and $2s2p^2$ for Ge XXVIII, Rb XXXIII, Sr XXXIV, Ru XL, Sn XLVI, and Ba LII using the GRASP2K code. The valence–valence (VV) and core–valence (CV) correlation effects are taken into account in a systematic way using active space approximation. Breit interactions and quantum electrodynamics (QED) effects are added in subsequent relativistic configuration interaction calculations. The accuracy of wavefunctions and calculated eigenvalues are assessed from the analysis of the convergence patterns and from the comparison with the available data. The ratio of the length to velocity forms of the transition rates (A_l/A_v) are also used to estimate the accuracy of our calculations. The calculated data will be useful for identifying fine structure levels and transition lines in further investigations.

2. Method of Calculation

2.1. Computational Procedure

The Grasp2K code [33] is based on the multi-configuration Dirac–Hartree–Fock (MCDHF) approach, taking relativistic and QED corrections into consideration. The MCDHF method has been described in detail by Grant [34]. We give a brief overview of the important features of the method.

The Dirac–Coulomb Hamiltonian is

$$H_{DC} = \sum_i (c\vec{\alpha}_i \cdot \vec{p}_i + (\beta_i - 1)c^2 + V_i^N) + \sum_{i>j} 1/r_{ij}. \quad (1)$$

The first term denotes the one-body contribution for an electron due to kinetic energy and interaction with the nucleus in JJ coupling. Here, α and β are 4×4 Dirac matrices, c denotes the speed of light, and V^N is the monopole part of the electron–nucleus coulomb interaction. The second term consists of the two-body Coulomb interactions between the electrons. The configuration state functions (CSFs) $\Phi(\Gamma_\alpha J^P)$ are formed by symmetry-adapted linear combinations of Slater determinants of the Dirac orbitals. Atomic state functions are then constructed by a linear combination of these atomic state functions (ASFs).

$$\Psi_i(J^P) = \sum_{\alpha=1}^{n_{csf}} C_{i\alpha}\Phi(\Gamma_\alpha J^P) \quad (2)$$

In the above equation, $C_{i\alpha}$ are mixing coefficients for the state i and n_{csf} denotes the number of CSFs used in the evaluation of ASFs. The one-electron and intermediate quantum numbers needed to define the CSFs are represented by Γ_α. The configuration mixing coefficients $C_{i\alpha}$ are obtained

through diagonalization of the Dirac–Coulomb Hamiltonian given in Equation (1). The radial parts of the Dirac orbitals and the expansion coefficients are optimized self-consistently in the relativistic self-consistent field procedure. After this, relativistic configuration interaction (RCI) calculations [35] can be performed. The most important transverse photon interaction included in the Hamiltonian

$$H_{Breit} = -\sum_{i<j}^{N} \left[\alpha_i \cdot \alpha_j \frac{\cos(w_{ij} r_{ij}/c)}{r_{ij}} + (\alpha_i \cdot \nabla_i)(\alpha_j \cdot \nabla_j) \frac{\cos(w_{ij} r_{ij}/c) - 1}{w_{ij}^2 r_{ij}/c^2} \right] \quad (3)$$

The contributions from the Breit interaction, vacuum polarization, self-energy, and finite nuclear mass corrections are added as first-order perturbation correction. The spin-angular part of the matrix elements is calculated using the second quantization method in coupled tensorial form and quasispin technique [36].

Transition Parameters

The transition parameters such as line strengths and rates for multipole transitions between two states $\psi_\alpha(PJM)$ and $\psi_\alpha(P'J'M')$ can be expressed in terms of the transition matrix element:

$$\left\langle \psi_\alpha(PJM) \,||\, Q_k^{(\lambda)} \,||\, \psi_\alpha(P'J'M') \right\rangle \quad (4)$$

Here $Q_k^{(\lambda)}$ denotes the corresponding transition operator of order k in Coulomb or Babushkin gauge [37]. Biorthogonal transformations of the atomic state functions were performed to compute the transition matrix element between two atomic state functions described by independently optimized orbital sets. Racah algebra techniques were used to evaluate the matrix element in the new representation.

2.2. Calculation Procedure

The extended optimal level (EOL) version of the MCDHF method is used to optimize the wave functions for all fine structure levels within a given term. In the EOL scheme [38], the optimization is on the weighted energy average of the states. The significant interactions between neighboring levels can be determined accurately in this method as simultaneous optimization of multiple levels with a specific J is performed in this method. We included different correlations in the calculation in a systematic approach; they are represented by the different constraints on the generation of CSFs included in Equation (2).The correlation between the valence electrons is defined as valence correlation (VV).In this, the core electrons are kept fixed and CSFs are generated by exciting valence electrons. The correlation between the valence electrons and core electrons is defined as core–valence correlation (CV), where one of the core electrons is excited to generate the CSFs. More than one core electron is allowed to excite in the core–core (CC) correlation, which is between the core electrons. We generated the CSFs using the active space approach [39,40]. This was done by exciting electrons from the reference configurations to a set of orbitals called the active set (AS).To generate configuration expansions for the fine structure terms belonging to the $2s^2 2p$ ground configuration, single and double substitutions (SD) were performed from the $\{2s^2 2p, 2p^3\}$ multireference set to an active set of orbitals. For the terms belonging to the $2s2p^2$ configuration, CSFs were generated by SD substitutions from the single reference configurations. By allowing excitations from a number of reference configurations to a set of relativistic orbitals, jj-coupled CSFs of particular parity and J symmetry were generated. We systematically enlarged the active sets to orbitals with principal quantum number $n = 3, \ldots, 7$ and orbital quantum numbers $l = 0, \ldots, 4$ (s,p,d,f,g) to observe the convergence.

$$\text{AS1} = \{n = 3, l = 0 - 2\}$$

Then, the active set is increased in the way shown:

$$\begin{aligned} \text{AS2} &= \text{AS1} + \{n = 4, \text{l} = 0-3\} \\ \text{AS3} &= \text{AS2} + \{n = 5, \text{l} = 0-4\} \\ \text{AS4} &= \text{AS3} + \{n = 6, \text{l} = 0-4\} \\ \text{AS5} &= \text{AS4} + \{n = 7, \text{l} = 0-4\}. \end{aligned}$$

Active set was increased in steps of orbital layers as orbitals with the same principal quantum number have similar energies. We optimized separately a set of orbitals for the even states and for the odd states.

In the present work, we included valence–valence (VV) and core–valence (CV) electron correlation effects to describe the inner properties. To reduce the processing time only the newly added orbitals were optimized. RCI (Relativistic Configuration Interaction) calculations including Breit interactions were performed to consider higher order correlation effects. Finally, the multireference sets for odd and even parity states were enlarged to include {$2s^2 2p$, $2p^3$, $2s2p3d$, $2p3d^2$} and {$2s2p^2$, $2p^2 3d$, $2s^2 3d$, $2s3d^2$}, respectively. The configurations with largest weights in the preceding self-consistent field calculations were included in the multireference set. To the final RCI calculations, QED effects (vacuum polarization and self-energy) were added as perturbation. The mixing coefficients obtained in the block structure format using MCDHF and RCI orbital wave functions were then reformed into non-block format and the initial and final state orbital wave functions were redesigned to a new form in which the two orbitals are biorthonormal [41,42]. These biorthonormal wavefunctions were then used to evaluate the dipole transition rates.

3. Results and Discussion

A very efficient way to ensure the convergence of atomic property within a certain correlation model is to use the active set approach to enlarge the configuration expansion systematically. We optimized the states of $2s^2 2p$, $2s2p^2$ configurations layer by layer. In order to consider VV correlations, calculations were performed with CSFs generated by single and double excitations from the 2s and 2p shells of the reference configurations $2s^2 2p$ and $2s2p^2$ to the active set. For CV calculations, we allow excitations from the 1s orbital also. Table 1 displays our computed level energies for 10 levels belonging to $2s^2 2p$ and $2s2p^2$ configurations of Ge XXVIII, Rb XXXIII, Sr XXXIV, Ru XL, Sn XLVI, and Ba LII as functions of the increasing active sets for VV and CV correlations. Energy contributions from Breit interaction and QED corrections are included in the calculations. For the odd parity states of Ge XXVIII, our RCI calculations included 182,470 and 6055 CSFs distributed over J = 1/2, 3/2 angular symmetries for the n = 7 results in the CV and VV correlations, respectively. For the even parity states, there were 277,127 and 10,546 CSFs distributed over J = 1/2, 3/2, and 5/2. Comparing our VV and CV calculations with other available data, we observe an improvement in the agreement when core orbital excitations are included. The computed energies for Rb XXXIII, Sr XXXIV, and Ba LII from CV correlation results agree well with the experimental values. The largest discrepancy between our computed energies from n = 7 CV calculations and National Institute of Standards and Technology (NIST) [43] values is 0.57% for $2s2p^2\,{}^2P_{1/2}$ level of Rb XXXIII. Further, we find our calculated energies are in good agreement with Koc [22] energy values. As Z increases, level ordering changes for some levels as seen from Table 1. For Ru XL, Sn XLVI and Ba LII, $2s2p^2\,{}^4P_{1/2}$ lies above $2s^2 2p\,{}^2P^{\circ}{}_{3/2}$ and for Sn XLVI and Ba LII, the levels $2s2p^2\,{}^4P_{5/2}$ and $2s2p^2\,{}^2D_{5/2}$ are interchanged.

The zero-order Dirac–Fock wave functions given by the reference configuration in the absence of electron correlation include limited number of configurations and hence are insufficient to represent the occupied orbitals. Therefore, more configurations must be added to represent electron correlations. The CSFs generated from these configurations must have same angular momentum and parity as the occupied orbital. In Table 2, we have presented the mixing coefficients for the wave functions of our

calculated levels. For instance, the configuration mixed wave function for the $2s2p^2\ ^4P_{1/2}$ level for Ge XXVIII is represented as

$$2s2p^2\ ^4P_{1/2} = 0.94\,2s2p^2(^4P_{1/2}) + 0.30\,2s2p^2(^2S_{1/2}) + 0.13\,2s2p^2\,(^2P_{1/2}),$$

where 0.94, 0.30 and 0.13 are the configuration mixing coefficients. The maximum contribution to the total wave function of a given level is from the same configuration. The contribution from each level is also listed in the table.

In Table 3, the radiative data for its $2s^22p\ ^2P^\circ_{1/2}$–$2s2p^2\ ^2D_{3/2}$ transition in Ge XXVIII are shown as functions of increasing active sets in VV and CV correlations. In both correlation calculations, the convergence of the results can be clearly seen as n increases. A good agreement between Coulomb and Babushkin gauges is found and this agreement improves with increasing n.

In Table 4, we have presented transition wavelengths as well as radiative rates, oscillator strengths, and line strengths for E1 (electric dipole) transitions from the ground state and first excited state for CV correlations. As CV results are better and converged fully, we have performed the calculations including CV correlation with $n = 7$. Results are provided in both Coulomb and Babushkin gauges. Both forms agree well as can be seen from Table 4, which indicates the accuracy of our results. A comparison between our computed transition wavelengths with NIST values [44] has been provided wherever possible and a good agreement achieved. The values of δT, which represents the deviation of ratio of length and velocity form of line strengths from unity and thus is an accuracy indicator, have also been tabulated. The maximum value of δT is 0.24, which confirms the accuracy of our results. In Figure 1 we have plotted transition wavelengths from ground state $2s^22p^2\ P^\circ_{1/2}$ to $2s2p^2\ ^4P_{1/2}$, $2s2p^2\ ^4P_{3/2}$, $2s2p^2\ ^2D_{3/2}$, $2s2p^2\ ^2P_{1/2}$, $2s2p^2\ ^2P_{3/2}$ and $2s2p^2\ ^2S_{1/2}$ levels as a function of Z. It is observed that wavelength decreases with increasing Z. The A_l/A_v values of E1 transitions from B-like ions for various Z are plotted in Figure 2. The ratios range from 0.90 to 1.01.The small discrepancy in the A_l and A_v values may be taken as a measure of the reliability of the computed rates. In Figures 3 and 4 we display the weighted oscillator strengths (gf) in length form for various E1 transitions from ground state as length form is considered more stable. For an allowed transition, the Z dependence depends on the Δj value. The jumping electron in such transition is either of type $2s_{1/2}$–$2p_{1/2}$ (Δj = 0) or $2s_{1/2}$–$2p_{3/2}$ (Δj = 1). For the B I sequence, the f value for an allowed transition (Δj = 1) increases slowly with Z while for transitions (Δj = 0) the f value decrease slowly with Z [45]. However, in the intermediate-Z region anti-crossings of the energy levels occur between two levels of same configuration, with the same J value having the same parity due to strong mixing in the corresponding wavefunctions. These states are nearly degenerate at a well-defined Z value. These anti-crossings of energy levels have a significant influence on the f value of the corresponding lines and can account for the anomalies in the systematic trends of the oscillator strengths involving the corresponding states.

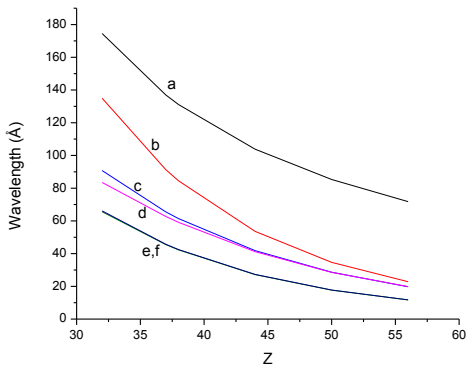

Figure 1. Transition wavelengths from ground state $2s^22p\ ^2P^\circ_{1/2}$ as a function of Z where curves a, b, c, d, e, f represent transitions to $2s2p^2\ ^4P_{1/2}$, $2s2p^2\ ^4P_{3/2}$, $2s2p^2\ ^2D_{3/2}$, $2s2p^2\ ^2P_{1/2}$, $2s2p^2\ ^2P_{3/2}$, and $2s2p^2\ ^2S_{1/2}$ levels, respectively.

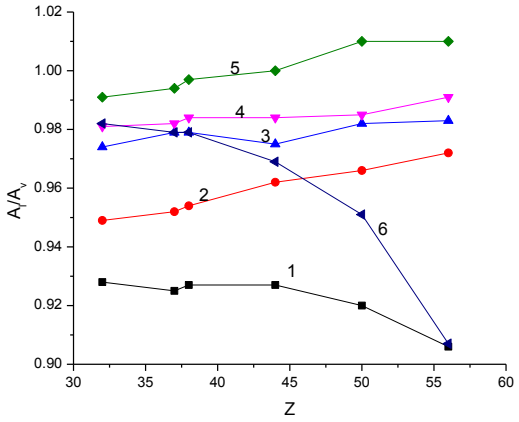

Figure 2. Ratios of length to velocity forms of rates for various transitions from $2s^2 2p\ ^2P^\circ_{1/2}$ state. Here 1, 2, 3, 4, 5, 6 represent transitions to $2s2p^2\ ^4P_{1/2}$, $2s2p^2\ ^4P_{3/2}$, $2s2p^2\ ^2D_{3/2}$, $2s2p^2\ ^2P_{1/2}$, $2s2p^2\ ^2P_{3/2}$, and $2s2p^2\ ^2S_{1/2}$ state, respectively.

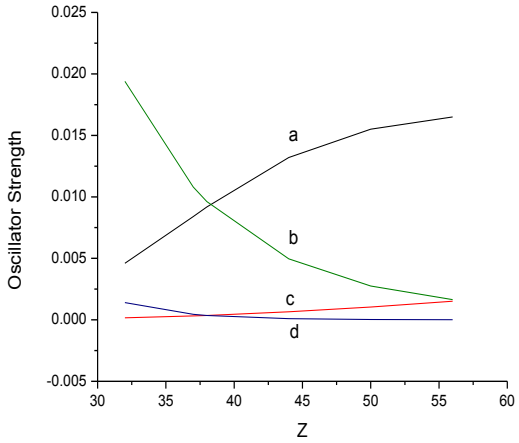

Figure 3. Weighted oscillator strengths (gf) as a function of Z. The curves a, b, c, d correspond to transitions to $2s2p^2\ ^4P_{1/2}$, $2s2p^2\ ^2P_{3/2}$, $2s2p^2\ ^4P_{3/2}$, $2s2p^2\ ^2S_{1/2}$ from $2s^2 2p\ ^2P^\circ_{1/2}$ state, respectively

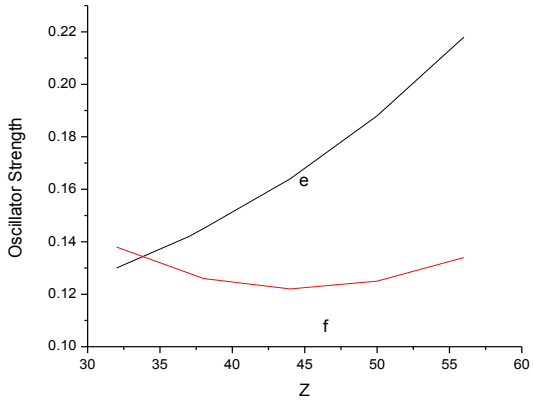

Figure 4. Weighted oscillator strengths (gf) as a function of Z. The curves e, and f correspond to transitions to $2s2p^2\ ^2D_{3/2}$, and $2s2p^2\ ^2P_{1/2}$ from $2s^2 2p\ ^2P^\circ_{1/2}$ state, respectively.

Table 1. Energies (in cm^{-1}) of fine-structure relativistic levels of Ge XXVIII, Rb XXXIII, Sr XXXIV, Ru XL, Sn XLVI, and Ba LII relative to ground state of B-like ions.

Ge										
Configuration	**VV**				**CV**					
	n = 4	**n = 5**	**n = 6**	**n = 7**	**n = 4**	**n = 5**	**n = 6**	**n = 7**	**Ref. [17]**	**Δ%**
$2s^2\ 2p\ ^2P^\circ_{1/2}$	0.00	0.00	0.00	0.00	0.00	0.00	0.00	0.00	0.00	0.00
$2s^2\ 2p\ ^2P^\circ_{3/2}$	294,359.19	294,335.58	294,358.61	294,371.64	294,445.85	294,544.84	294,700.43	294,824.39	294,539	0.09
									294,658[a]	0.06
									294,668[b]	0.05
									294,550[c]	0.09
									294,614[d]	0.07
$2s2p^2\ ^4P_{1/2}$	572,810.09	573,172.37	573,274.34	573,321.06	572,252.78	572,596.33	572,794.37	572,943.86	574,559	0.28
									573,139[a]	0.03
									572,858[b]	0.01
$2s2p^2\ ^4P_{3/2}$	740,529.66	740,925.26	741,020.59	741,066.48	740,080.93	740,426.04	740,591.13	740,721.62	742,598	0.25
$2s2p^2\ ^4P_{5/2}$	846,036.05	846,212.79	846,272.93	846,303.89	845,542.28	845,510.69	845,513.03	845,531.07	847,406	0.22
$2s2p^2\ ^2D_{3/2}$	1,103,153.70	1,102,793.77	1,102,766.60	1,102,760.55	1,102,276.49	1,101,807.99	1,101,836.13	1,101,909.39	1,102,111	0.02
$2s2p^2\ ^2P_{1/2}$	1,199,600.45	1,199,379.88	1,199,412.07	1,199,425.53	1197969.03	1197600.77	1,197,678.13	1,197,770.15	1,197,323	0.04
$2s2p^2\ ^2D_{5/2}$	1,211,205.85	1,210,750.86	1,210,686.99	1,210,664.84	1,210,505.67	1,209,856.50	1,209,748.39	1,209,723.04	1,211,608	0.15
$2s2p^2\ ^2S_{1/2}$	1,513,917.87	1,513,582.64	1,513,577.79	1,513,573.67	1,512,905.95	1,512,529.92	1,512,614.73	1,512,712.55	1,505,579	0.47
$2s2p^2\ ^2P_{3/2}$	1,527,073.63	1,526,714.16	1,526,697.23	1,526,695.12	1525292.77	1524737.12	1,524,740.20	1,524,799.94	1,523,491	0.08
Rb										
Configuration	**VV**				**CV**					
	n = 4	**n = 5**	**n = 6**	**n = 7**	**n = 4**	**n = 5**	**n = 6**	**n = 7**	**Other**	**Δ%**
$2s^22p\ ^2P^\circ_{1/2}$	0.00	0.00	0.00	0.00	0.00	0.00	0.00	0.00	0.00	0.00
$2s^22p\ ^2P^\circ_{3/2}$	554,879.16	554,870.27	554,891.60	554,907.79	554,994.57	555,105.27	555,259.44	555,379.85	554,700[c]	0.12
									555,329[a]	0.01
									555,338[b]	0.01
$2s2p^2\ ^4P_{1/2}$	730,395.31	730,657.17	730,740.17	730,781.53	729,723.78	729,940.10	730,109.73	730,241.58	726,900[c]	0.46
									730,429[a]	0.02
									730,041[b]	0.03
$2s2p^2\ ^4P_{3/2}$	1,095,432.10	1,095,811.16	1,095,900.17	1,095,946.77	1,094,951.96	1,095,471.35	1,095,401.41	1,095,517.75	1,089,900[c]	0.51
$2s2p^2\ ^4P_{5/2}$	1,245,199.88	1,245,245.18	1,245,275.42	1,245,296.70	1,244,612.54	1,244,431.32	1,244,402.22	1,244,404.33	1,242,100[c]	0.18
$2s2p^2\ ^2D_{3/2}$	1,527,957.94	1,527,589.89	1,527,553.99	1,527,548.25	1,527,778.22	1,526,581.58	1,526,417.03	1,526,473.27	1,532,900[c]	0.42
$2s2p^2\ ^2P_{1/2}$	1,597,246.42	1,597,079.83	1,597,124.78	1,597,147.92	1,595,466.01	1,595,131.27	1,595,213.20	1,595,303.30	1,604,400[c]	0.57
$2s2p^2\ ^2D_{5/2}$	1,814,677.32	1,814,403.75	1,814,366.82	1,814,358.66	1,814,002.12	1,813,535.33	1,813,459.03	1,813,444.10	1,814,700[c]	0.07
$2s2p^2\ ^2S_{1/2}$	2,187,867.67	2,187,546.02	2,187,542.46	2,187,542.52	2,186,881.54	2,186,524.70	2,186,614.52	2,186,711.39	2,191,200[c]	0.20
$2s2p^2\ ^2P_{3/2}$	2,199,518.57	2,199,195.73	2,199,184.27	2,199,188.43	2,198,582.20	2,197,311.71	2,197,213.85	2,197,269.66	2,207,900[c]	0.48

Table 1. *Cont.*

Sr										
Configuration	**VV**				**CV**					
	n = 4	**n = 5**	**n = 6**	**n = 7**	**n = 4**	**n = 5**	**n = 6**	**n = 7**	**Other**	**Δ%**
$2s^2 2p\ ^2P^\circ_{1/2}$	0.00	0.00	0.00	0.00	0.00	0.00	0.00	0.00	0.00	0.00
$2s^2 2p\ ^2P^\circ_{3/2}$	623,284.03	623,275.74	623,301.64	623,316.67	623,405.36	623,519.82	623,675.76	623,379.36	623,100[c]	0.04
									623,739[a]	0.06
									623,747[b]	0.06
$2s2p^2\ ^4P_{1/2}$	763,024.73	763,262.18	763,345.64	763,384.59	762,324.87	762,514.86	762,679.97	762,807.35	759,800[c]	0.39
									762,976[a]	0.02
									762,565[b]	0.03
$2s2p^2\ ^4P_{3/2}$	1,183,539.38	1,183,909.04	1,184,000.99	1,184,046.38	1,183,036.48	1,183,318.82	1,183,448.77	1,183,551.33	1,178,000[c]	0.47
$2s2p^2\ ^4P_{5/2}$	1,341,468.23	1,341,487.09	1,341,515.58	1,341,534.53	1,340,860.77	1,340,652.95	1,340,618.81	1,340,617.83	1,338,600[c]	0.15
$2s2p^2\ ^2D_{3/2}$	1,629,937.45	1,629,540.42	1,629,503.96	1,629,495.58	1,628,859.19	1,628,304.40	1,628,288.42	1,628,331.20	1,634,900[c]	0.40
$2s2p^2\ ^2P_{1/2}$	1,693,721.64	1,693,562.92	1,693,614.61	1,693,638.49	1,691,914.66	1,691,588.56	1,691,673.26	1,691,762.37	1,700,800[c]	0.53
$2s2p^2\ ^2D_{5/2}$	1,969,084.81	1,968,840.72	1,968,812.81	1,968,807.12	1,968,414.67	1,967,981.54	1,967,912.63	1,967,900.11	1,968,800[c]	0.04
$2s2p^2\ ^2S_{1/2}$	2,355,943.75	2,355,623.32	2,355,624.88	2,355,624.75	2,354,959.94	2,354,609.24	2,354,702.02	2,354,798.15	2,359,100[c]	0.18
$2s2p^2\ ^2P_{3/2}$	2,367,421.82	2,367,072.08	2,367,061.00	2,367,063.13	2,365,622.03	2,365,064.97	2,365,055.70	2,365,100.13	2,375,500[c]	0.44
Ru										
Configuration	**VV**				**CV**					
	n = 4	**n = 5**	**n = 6**	**n = 7**	**n = 4**	**n = 5**	**n = 6**	**n = 7**	**Ref. [23]**	**Δ%**
$2s^2 2p\ ^2P^\circ_{1/2}$	0.00	0.00	0.00	0.00	0.00	0.00	0.00	0.00		0.00
$2s2p^2\ ^4P_{1/2}$	963,735.96	963,847.87	963,910.53	963,929.75	962,833.63	962,867.47	962,993.35	963,105.03	963,285[a]	0.02
									962,734[b]	0.04
$2s^2 2p\ ^2P^\circ_{3/2}$	1,180,758.61	1,180,767.78	1,180,797.79	1,180,804.10	1,180,916.59	1,181,063.55	1,181,219.58	1,181,344.53	1,181,453[a]	0.01
									1,181,450[b]	0.01
$2s2p^2\ ^4P_{3/2}$	1,865,365.70	1,865,718.29	1,865,804.50	1,865,836.54	1,864,874.29	1,865,056.33	1,865,163.52	1,865,257.38		
$2s2p^2\ ^4P_{5/2}$	2,066,640.94	2,066,553.94	2,066,559.15	2,066,556.66	2,065,913.40	2,065,586.26	2,065,510.67	2,065,498.15		
$2s2p^2\ ^2D_{3/2}$	2,393,724.80	2,393,327.09	2,393,285.00	2,393,262.22	2,392,484.98	2,391,858.98	2,391,815.83	2,391,847.82		
$2s2p^2\ ^2P_{1/2}$	2,428,031.86	2,427,931.61	2,427,998.54	2,428,019.48	2,426,075.45	2,425,798.57	2,425,886.93	2,425,980.87		
$2s2p^2\ ^2D_{5/2}$	3,199,253.57	3,199,167.00	3,199,170.59	3,199,166.72	3,198,607.59	3,198,345.46	3,198,301.12	3,198,306.13		
$2s2p^2\ ^2S_{1/2}$	3,665,385.67	3,665,095.71	3,665,106.49	3,665,100.75	3,664,395.96	3,465,296.95	3,465,029.12	3,464,957.16		
$2s2p^2\ ^2P_{3/2}$	3,676,012.00	3,675,708.30	3,675,706.90	3,675,701.93	3,674,204.06	3,664,086.23	3,664,186.22	3,664,289.99		

Table 1. *Cont.*

Configuration	VV				CV					
	n = 4	**n = 5**	**n = 6**	**n = 7**	**n = 4**	**n = 5**	**n = 6**	**n = 7**	**Ref. [23]**	**Δ%**
Sn										
$2s^2 2p\ ^2P^\circ_{1/2}$	0.00	0.00	0.00	0.00	0.00	0.00	0.00	0.00		0.00
$2s2p^2\ ^4P_{1/2}$	1,172,932.39	1,172,931.39	1,172,977.25	1,173,002.49	1,171,793.52	1,171,681.51	1,171,782.28	1,171,874.84	1,172,053[a]	0.01
									1,171,358[b]	0.04
$2s^2 2p\ ^2P^\circ_{3/2}$	2,063,472.21	2,063,518.86	2,063,547.86	2,063,572.30	2,063,683.87	2,063,868.26	2,064,045.18	2,064,175.01	2,064,478[a]	0.01
									2,064,448[b]	0.01
$2s2p^2\ ^4P_{3/2}$	2,884,412.96	2,884,756.24	2,884,839.77	2,884,884.61	2,883,794.52	2,884,027.38	2,884,133.52	2,884,220.49		
$2s2p^2\ ^2D_{5/2}$	3,121,078.42	3,120,936.00	3,120,931.84	3,120,935.40	3,120,228.30	3,119,821.85	3,119,731.04	3,119,706.80		
$2s2p^2\ ^2D_{3/2}$	3,493,429.54	3,493,073.93	3,493,038.56	3,493,033.78	3,491,945.09	3,491,391.15	3,491,352.02	3,491,378.27		
$2s2p^2\ ^2P_{1/2}$	3,505,894.95	3,505,837.96	3,505,919.22	3,505,960.42	3,503,775.07	3,503,534.71	3,503,638.30	3,503,732.41		
$2s2p^2\ ^4P_{5/2}$	5,096,696.59	5,096,720.50	5,096,752.03	5,096,771.52	5,096,062.17	4,761,571.79	4,761,262.07	4,761,169.15		
$2s2p^2\ ^2S_{1/2}$	5,640,312.35	5,640,057.95	5,640,081.85	5,640,096.00	5,639,304.58	5,095,918.02	5,095,910.46	5,095,927.34		
$2s2p^2\ ^2P_{3/2}$	5,650,330.14	5,650,123.49	5,650,145.57	5,650,165.52	5,648,454.69	5,639,044.37	5,639,168.23	5,639,277.45		
Ba										
Configuration	**VV**				**CV**					
	n = 4	**n = 5**	**n = 6**	**n = 7**	**n = 4**	**n = 5**	**n = 6**	**n = 7**	**Ref. [23]**	**Δ%**
$2s^2 2p\ ^2P^\circ_{1/2}$	0.00	0.00	0.00	0.00	0.00	0.00	0.00	0.00		
$2s2p^2\ ^4P_{1/2}$	1,394,480.97	1,394,373.83	1,394,398.45	1,394,422.04	1,393,070.22	1,392,820.60	1,392,896.06	1,392,944.14		
									1,393,276[a]	0.02
									1,392,459[b]	0.03
$2s^2 2p\ ^2P^\circ_{3/2}$	3,393,333.19	3,393,412.40	3,393,454.03	3,393,489.63	3,393,607.70	3,393,850.70	3,394,049.82	3,394,191.00		
									3,394,759[a]	0.02
									3,394,676[b]	0.01
$2s2p^2\ ^4P_{3/2}$	4,365,092.43	4,365,428.44	4,365,506.06	4,365,555.28	4,364,405.03	4,364,626.73	4,364,728.87	4,364,816.11		
$2s2p^2\ ^2D_{5/2}$	4,631,483.73	4,631,314.92	4,631,300.47	4,631,309.82	4,630,674.88	4,630,045.47	4,629,940.55	4,629,909.23		
$2s2p^2\ ^2P_{1/2}$	5,052,120.83	5,052,094.24	5,052,183.32	5,052,236.95	5,049,800.11	5,049,589.51	5,049,709.12	5,049,720.16		
$2s2p^2\ ^2D_{3/2}$	5,054,465.27	5,054,148.70	5,054,121.67	5,054,125.23	5,052,767.66	5,052,245.40	5,052,210.60	5,052,239.37		
$2s2p^2\ ^4P_{5/2}$	7,905,439.73	7,905,551.78	7,905,601.74	7,905,639.21	7,904,940.53	6,535,783.59	6,535,433.14	6,535,318.45		
$2s2p^2\ ^2S_{1/2}$	8,528,078.13	8,527,865.22	8,527,899.71	8,527,927.19	8,527,043.94	7,904,769.39	7,904,793.46	7,904,826.22		
$2s2p^2\ ^2P_{3/2}$	8,537,396.20	8,537,283.19	8,537,328.52	8,537,364.66	8,535,451.45	8,526,851.59	8,527,006.46	8,527,195.97		

Theory – DHF[a]: [a] QED corrections estimated from hydrogenic self-energy [23];
Theory – DHF [b]: [b] QED corrections from screened model [23]
[c]: NIST [43]; Δ% : $\frac{|MCDHF-Others|}{Others} \times 100$
[d]: Ref. [29]

Table 2. The configuration mixing coefficients and contributions for levels in B-like ions. The number in parenthesis refers to the level number.

Ge		
Level	**Mix**	**Contribution**
$2s^2 2p\ ^2P^\circ_{1/2}$	0.99 (1) + 0.12 ($2p^3\ ^2P^\circ_{1/2}$)	0.98 (1) + 0.01 ($2p^3\ ^2P^\circ_{1/2}$)
$2s^2 2p\ ^2P^\circ_{3/2}$	0.99 (2) + 0.14 ($2p^3\ ^2P^\circ_{3/2}$)	0.98 (2) + 0.02 ($2p^3\ ^2P^\circ_{3/2}$)
$2s2p^2\ ^4P_{1/2}$	0.94 (3) + 0.30 (9) + 0.13 (7)	0.89 ($2s2p^2\ ^4P_{1/2}$) + 0.09 (9) + 0.02 (7)
$2s2p^2\ ^4P_{3/2}$	–0.99 (4) + 0.11 (6)+ 0.08 (10)	–0.99 (4) + 0.11 (6) + 0.08 (10)
$2s2p^2\ ^4P_{5/2}$	0.90 (5) – 0.43 (8)	0.81 (5) + 0.19 (8)
$2s2p^2\ ^2D_{3/2}$	0.93 (6) + 0.34 (10) + 0.08 (4)	0.87 (6) + 0.12 (10) + 0.01 (4)
$2s2p^2\ ^2P_{1/2}$	0.84 (7) + 0.47 (9) + 0.27 (3)	0.70 (7) + 0.22 (9) + 0.07 (3)
$2s2p^2\ ^2D_{5/2}$	0.90(8) + 0.43 (5)	0.81 (8) + 0.19 (5)
$2s2p^2\ ^2S_{1/2}$	0.82 (9) – 0.52 (7) – 0.19(3)	0.69 (9) + 0.27 (7) + 0.04 (3)
$2s2p^2\ ^2P_{3/2}$	0.93 (10) – 0.33 (6) – 0.11 (4)	0.87 ($2s2p^2\ ^2P_{3/2}$) + 0.11 (6) + 0.01 (4)
Rb		
Level	**Mix**	**Contribution**
$2s^2 2p\ ^2P^\circ_{1/2}$	0.99 (1) + 0.11 ($2p^3\ ^2P^\circ_{1/2}$)	0.99 (1) + 0.01($2p^3\ ^2P^\circ_{1/2}$)
$2s^2 2p\ ^2P^\circ_{3/2}$	0.99 (2) + 0.14 ($2p^3\ ^2P^\circ_{3/2}$)	0.98 (2) + 0.02 ($2p^3\ ^2P^\circ_{3/2}$)
$2s2p^2\ ^4P_{1/2}$	0.90 (3) + 0.39 (9) + 0.20 (7)	0.80 (3) + 0.15 (9) + 0.04 (7)
$2s2p^2\ ^4P_{3/2}$	–0.98 (4) + 0.15 (6) – 0.10 (10)	0.97 (4) + 0.02 (6) + 0.01 (10)
$2s2p^2\ ^4P_{5/2}$	0.82 (5) – 0.57 (8)	0.67 (5) + 0.32 (8)
$2s2p^2\ ^2D_{3/2}$	0.90 (6) + 0.43 (10) +0.09 (4)	0.80 (6) + 0.19 (10) +0.01 (4)
$2s2p^2\ ^2P_{1/2}$	0.85 (7) +0.37 (9) – 0.36 (3)	0.73 (7) + 0.14 (9) + 0.13 (3)
$2s2p^2\ ^2D_{5/2}$	0.82 (8) + 0.57(5)	0.67(8) + 0.32 (5)
$2s2p^2\ ^2S_{1/2}$	0.84 (9) – 0.47 (7) – 0.25 (3)	0.77 (9) + 0.22 (7) + 0.07 (3)
$2s2p^2\ ^2P_{3/2}$	0.89 (10) – 0.41 (6) – 0.16 (4)	0.80 (10) + 0.17 (6) + 0.02 (4)
Sr		
Level	**Mix**	**Contribution**
$2s^2 2p\ ^2P^\circ_{1/2}$	0.99 (1) + 0.10 ($2p^3\ ^2P^\circ_{1/2}$)	0.99 (1) + 0.01 ($2p^3\ ^2P^\circ_{1/2}$)
$2s^2 2p\ ^2P^\circ_{3/2}$	0.99 (2) + 0.13 ($2p^3\ ^2P^\circ_{3/2}$)	0.98(2) + 0.02 ($2p^3\ ^2P^\circ_{3/2}$)
$2s2p^2\ ^4P_{1/2}$	0.89 (3) + 0.41 (9) + 0.22 (7)	0.78 (3) + 0.16 (9) + 0.05 (7)
$2s2p^2\ ^4P_{3/2}$	–0.98 (4) + 0.16 (6) – 0.11 (10)	0.96 (4) + 0.02 (6) – 0.01 (10)
$2s2p^2\ ^4P_{5/2}$	0.80 (5) – 0.59 (8)	0.65(5) + 0.35 (8)
$2s2p^2\ ^2D_{3/2}$	0.89 (6) – 0.43 (10) – 0.16 (4)	0.79 (6) + 0.20 (10) +0.01 (4)
$2s2p^2\ ^2P_{1/2}$	0.86 (7) – 0.37 (3) + 0.35 (9)	0.73 (7) – 0.14 (3) + 0.12 (9)
$2s2p^2\ ^2D_{5/2}$	0.80 (8) + 0.59 (5)	0.65 (8) + 0.35(5)
$2s2p^2\ ^2S_{1/2}$	0.84 (9) – 0.46 (7) – 0.27 (3)	0.71 (9) + 0.21 (7) + 0.07 (3)
$2s2p^2\ ^2P_{3/2}$	0.89 (10) – 0.43 (6) – 0.16 (4)	0.79 (10) + 0.18 (6) + 0.03 (4)

Table 2. *Cont.*

Ru		
Level	**Mix**	**Contribution**
$2s^2 2p\ ^2P^\circ_{1/2}$	0.99 (1) + 0.08 ($2p^3\ ^2P^\circ_{1/2}$)	0.99 (1) + 0.01 ($2p^3\ ^2P^\circ_{1/2}$)
$2s^2 2p\ ^2P^\circ_{3/2}$	0.99 (2) + 0.12 ($2p^3\ ^2P^\circ_{3/2}$)	0.98(2) + 0.01 ($2p^3\ ^2P^\circ_{3/2}$)
$2s2p^2\ ^4P_{1/2}$	0.83 (3) + 0.47 (9) + 0.30 (7)	0.69 (3) + 0.22 (9) + 0.09 (7)
$2s2p^2\ ^4P_{3/2}$	–0.97 (4) + 0.19 (6) – 0.13 (10)	0.95 (4) + 0.04 (6) + 0.02 (10)
$2s2p^2\ ^4P_{5/2}$	0.73(5) – 0.68 (8)	0.53 (5) + 0.47 (8)
$2s2p^2\ ^2D_{3/2}$	0.85 (6) – 0.51 (10) – 0.10 (4)	0.73 (6) + 0.26 (10) +0.01 (4)
$2s2p^2\ ^2P_{1/2}$	0.85 (7) – 0.45 (3) + 0.25 (9)	0.73 (7) + 0.20 (3) +0.06 (9)
$2s2p^2\ ^2D_{5/2}$	0.73(8) + 0.68 (5)	0.53 (8) + 0.47 (5)
$2s2p^2\ ^2S_{1/2}$	0.84 (9) – 0.42 (7) – 0.33 (3)	0.71 (9) + 0.18 (7) + 0.11 (3)
$2s2p^2\ ^2P_{3/2}$	0.85 (10) – 0.48 (6) – 0.21 (4)	0.72 (10) + 0.24 (6) + 0.04 (4)
Sn		
Level	**Mix**	**Contribution**
$2s^2 2p\ ^2P^\circ_{1/2}$	0.99 (1) + 0.07 ($2p^3\ ^2P^\circ_{1/2}$)	0.99 (1) + 0.00 ($2p^3\ ^2P^\circ_{1/2}$)
$2s^2 2p\ ^2P^\circ_{3/2}$	0.99 (2) + 0.11 ($2p^3\ ^2P^\circ_{3/2}$)	0.98 (2) + 0.01 ($2p^3\ ^2P^\circ_{3/2}$)
$2s2p^2\ ^4P_{1/2}$	0.78 (3) + 0.51 (9) + 0.35 (7)	0.61 (3) + 0.26 (9) + 0.12 (7)
$2s2p^2\ ^4P_{3/2}$	–0.96 (4) + 0.22 (6) – 0.14 (10)	0.93 (4) + 0.05 (6) + 0.02 (10)
$2s2p^2\ ^2D_{5/2}$	–0.73 (5) + 0.68 (8)	0.54 (5) + 0.46 (8)
$2s2p^2\ ^2D_{3/2}$	0.83 (6) – 0.55 (10) + 0.10 (4)	0.68 (6) + 0.31 (10) + 0.01 (4)
$2s2p^2\ ^2P_{1/2}$	0.85 (7) – 0.50 (3) + 0.18 (9)	0.72 (7) + 0.25 (3) + 0.03 (9)
$2s2p^2\ ^4P_{5/2}$	0.73 (8) + 0.68 (5)	0.54 (8) + 0.46 (5)
$2s2p^2\ ^2S_{1/2}$	0.84 (9) – 0.40 (7) – 0.37 (3)	0.70 (9) + 0.16 (7) + 0.14 (3)
$2s2p^2\ ^2P_{3/2}$	0.82 (10) – 0.52 (6) – 0.24 (4)	0.67(10) + 0.27 (6) + 0.06 (4)
Ba		
Level	**Mix**	**Contribution**
$2s^2 2p\ ^2P^\circ_{1/2}$	0.99 (1) + 0.05 ($2p^3\ ^2P^\circ_{1/2}$)	0.99 (1) + 0.00($2p^3\ ^2P^\circ_{1/2}$)
$2s^2 2p\ ^2P^\circ_{3/2}$	0.99 (2) + 0.11 ($2p^3\ ^2P^\circ_{3/2}$)	0.98 (2) + 0.01 ($2p^3\ ^2P^\circ_{3/2}$)
$2s2p^2\ ^4P_{1/2}$	0.73 (3) + 0.53 (9) +0.38 (7)	0.56 (3) + 0.28 (9) +0.14 (7)
$2s2p^2\ ^4P_{3/2}$	–0.96 (4) + 0.27 (6) – 0.16 (10)	0.92 (4) +0.05 (6) + 0.02 (10)
$2s2p^2\ ^2D_{5/2}$	–0.76(5) + 0.64 (8)	0.58 (5) + 0.42 (8)
$2s2p^2\ ^2D_{3/2}$	0.81 (6) + 0.58 (10) + 0.10 (4)	0.65 (6) + 0.33 (10) + 0.01 (4)
$2s2p^2\ ^2P_{1/2}$	0.84 (7) – 0.52 (3) + 0.13 (9)	0.71 (7) + 0.27 (3) + 0.02 (9)
$2s2p^2\ ^4P_{5/2}$	0.76 (8) + 0.64 (5)	0.58 (8) + 0.42 (5)
$2s2p^2\ ^2S_{1/2}$	0.83 (9) – 0.40 (3) – 0.38 (7)	0.70 (9) + 0.16 (3) + 0.14 (7)
$2s2p^2\ ^2P_{3/2}$	0.80 (10) – 0.54 (6) – 0.26 (4)	0.64(10) + 0.29 (6) + 0.07 (4)

Table 3. Convergence of the radiative data and transition energy between the $2s^2 2p\ ^2P^{\circ}_{1/2}$ and $2s2p^2\ ^2D_{3/2}$ levels of B-like Ge.

VV									
Active set	**λ (in Å)**	**A**		**gf**		**S**			**Δ*E* (cm^{-1})**
n		**B**	**C**	**B**	**C**	**B**	**C**	**S_l/S_v**	
3	90.35	2.67E+10	2.96E+10	1.31E−01	1.45E−01	3.89E−02	4.31E−02	0.902	1106813
4	90.65	2.64E+10	2.84E+10	1.30E−01	1.40E−01	3.88E−02	4.18E−02	0.928	1103153
5	90.68	2.63E+10	2.85E+10	1.30E−01	1.41E−01	3.88E−02	4.20E−02	0.924	1102793
6	90.68	2.63E+10	2.85E+10	1.30E−01	1.41E−01	3.88E−02	4.20E−02	0.924	1102766
7	90.68	2.63E+10	2.85E+10	1.30E−01	1.41E−01	3.88E−02	4.20E−02	0.924	1102760
	90.73[e]								1102111[e]
CV									
Active set	**λ (in Å)**	**A**		**gf**		**S**			**Δ*E* (cm^{-1})**
n		**B**	**C**	**B**	**C**	**B**	**C**	**S_l/S_v**	
3	90.37	2.67E+10	2.83E+10	1.31E−01	1.39E−01	3.89E−02	4.12E−02	0.944	1106581
4	90.72	2.63E+10	2.68E+10	1.30E−01	1.32E−01	3.87E−02	3.96E−02	0.977	1102276
5	90.76	2.62E+10	2.69E+10	1.30E−01	1.33E−01	3.87E−02	3.96E−02	0.977	1101807
6	90.76	2.62E+10	2.69E+10	1.30E−01	1.33E−01	3.87E−02	3.96E−02	0.977	1101836
7	90.75	2.62E+10	2.69E+10	1.30E−01	1.33E−01	3.87E−02	3.96E−02	0.977	1101909
	90.73[e]								1102111[e]

e: Ref. [17]

Table 4. Transition data for E1 transitions for B-like ions from $2s^2 2p\ ^2P^\circ_{1/2,\,3/2}$: lower level i, upper level j, wavelength λ (in Å), transition rate A (s^{-1}), weighted oscillator strength gf, line strength S (in a.u), and accuracy indicator (dT).

Ge										
Transition		**λ (in Å)**	**λ_c (in Å) Ref. [17]**	**A**		**gf**		**S**		**dT**
i	**j**			**B**	**C**	**B**	**C**	**B**	**C**	
$2s^2\ 2p\ ^2P^\circ_{1/2}$	$2s2p^2\ ^4P_{1/2}$	174.54	174.05	5.04E+08	5.43E+08	4.60E−03	4.96E−03	2.64E−03	2.85E−03	0.0719
$2s^2\ 2p\ ^2P^\circ_{1/2}$	$2s2p^2\ ^4P_{3/2}$	135.00	134.66	1.49E+07	1.57E+07	1.63E−04	1.72E−04	7.24E−05	7.65E−05	0.0539
$2s^2\ 2p\ ^2P^\circ_{1/2}$	$2s2p^2\ ^2D_{3/2}$	90.75	90.735	2.62E+10	2.69E+10	1.30E−01	1.33E−01	3.87E−02	3.96E−02	0.0233
$2s^2\ 2p\ ^2P^\circ_{1/2}$	$2s2p^2\ ^2P_{1/2}$	83.49	83.520	6.62E+10	6.75E+10	1.38E−01	1.41E−01	3.80E−02	3.87E−02	0.0188
$2s^2\ 2p\ ^2P^\circ_{1/2}$	$2s2p^2\ ^2P_{3/2}$	65.58	65.639	7.51E+09	7.58E+09	1.94E−02	1.95E−02	4.18E−03	4.22E−03	0.0086
$2s^2\ 2p\ ^2P^\circ_{1/2}$	$2s2p^2\ ^2S_{1/2}$	66.11	66.420	1.07E+09	1.09E+09	1.40E−03	1.43E−03	3.06E−04	3.12E−04	0.0199
$2s^2\ 2p\ ^2P^\circ_{3/2}$	$2s2p^2\ ^4P_{1/2}$	359.56	357.12	1.57E+07	1.73E+07	6.08E−04	6.73E−04	7.20E−04	7.96E−04	0.0953
$2s^2\ 2p\ ^2P^\circ_{3/2}$	$2s2p^2\ ^4P_{3/2}$	224.27	223.18	3.19E+07	3.62E+07	9.64E−04	10.91E−04	7.12E−04	8.06E−04	0.1170
$2s^2\ 2p\ ^2P^\circ_{3/2}$	$2s2p^2\ ^4P_{5/2}$	181.58	180.88	4.23E+08	4.58E+08	1.25E−02	1.36E−02	7.50E−03	8.12E−03	0.0763
$2s^2\ 2p\ ^2P^\circ_{3/2}$	$2s2p^2\ ^2D_{3/2}$	123.90	123.83	1.67E+08	1.78E+08	1.54E−03	1.64E−03	6.29E−04	6.70E−04	0.0612
$2s^2\ 2p\ ^2P^\circ_{3/2}$	$2s2p^2\ ^2P_{1/2}$	110.75	110.77	1.07E+09	1.13E+09	3.95E−03	4.17E−03	1.44E−03	1.52E−03	0.0543
$2s^2\ 2p\ ^2P^\circ_{3/2}$	$2s2p^2\ ^2D_{5/2}$	109.30	109.04	9.64E+09	9.88E+09	2.39E+00	2.39E+00	5.93E−02	5.93E−02	0.0008
$2s^2\ 2p\ ^2P^\circ_{3/2}$	$2s2p^2\ ^2S_{1/2}$	82.11	82.574	5.63E+10	5.68E+10	1.14E−01	1.15E−01	3.07E−02	3.10E−02	0.0090
$2s^2\ 2p\ ^2P^\circ_{3/2}$	$2s2p^2\ ^2P_{3/2}$	81.30	81.370	7.83E+10	7.92E+10	3.10E−01	3.14E−01	8.31E−02	8.40E−02	0.0111
Rb										
Transition		**λ(in Å)**	**λ_c (in Å) NIST [44]**	**A**		**gf**		**S**		**dT**
i	**j**			**B**	**C**	**B**	**C**	**B**	**C**	
$2s^2 2p\ ^2P^\circ_{1/2}$	$2s2p^2\ ^4P_{1/2}$	136.94	137.571	1.49E+09	1.61E+09	8.40E−03	9.04E−03	3.79E−03	4.07E−03	0.0702
$2s^2 2p\ ^2P^\circ_{1/2}$	$2s2p^2\ ^4P_{3/2}$	91.28	91.752	6.38E+07	6.70E+07	3.19E−04	3.35E−04	9.59E−05	10.05E−05	0.0467
$2s^2 2p\ ^2P^\circ_{1/2}$	$2s2p^2\ ^2D_{3/2}$	65.51	65.236	5.52E+10	5.64E+10	1.42E−01	1.45E−01	3.06E−02	3.13E−02	0.0216
$2s^2 2p\ ^2P^\circ_{1/2}$	$2s2p^2\ ^2P_{1/2}$	62.68	62.329	1.09E+11	1.11E+11	1.28E−01	1.30E−01	2.64E−02	2.69E−02	0.0182
$2s^2 2p\ ^2P^\circ_{1/2}$	$2s2p^2\ ^2P_{3/2}$	45.51	45.292	8.69E+09	8.74E+09	1.08E−02	1.08E−02	1.62E−03	1.63E−03	0.0049
$2s^2 2p\ ^2P^\circ_{1/2}$	$2s2p^2\ ^2S_{1/2}$	45.73	45.637	7.09E+08	7.24E+08	4.44E−04	4.54E−04	6.69E−05	6.84E−05	0.0215
$2s^2 2p\ ^2P^\circ_{3/2}$	$2s2p^2\ ^4P_{1/2}$	571.88	580.720	3.54E+06	4.19E+06	3.47E−04	4.10E−04	6.53E−04	7.73E−04	0.1547
$2s^2 2p\ ^2P^\circ_{3/2}$	$2s2p^2\ ^4P_{3/2}$	185.14	186.846	7.22E+07	8.19E+07	1.48E−03	1.68E−03	9.04E−04	10.26E−04	0.1185
$2s^2 2p\ ^2P^\circ_{3/2}$	$2s2p^2\ ^4P_{5/2}$	145.13	145.476	1.07E+09	1.17E+09	2.03E−02	2.21E−02	9.72E−03	1.06E−02	0.0806
$2s^2 2p\ ^2P^\circ_{3/2}$	$2s2p^2\ ^2D_{3/2}$	102.98	102.229	8.86E+08	9.35E+08	5.63E−03	5.94E−03	1.91E−03	2.01E−03	0.0522
$2s^2 2p\ ^2P^\circ_{3/2}$	$2s2p^2\ ^2P_{1/2}$	96.16	95.265	2.38E+09	2.52E+09	6.59E−03	6.98E−03	2.09E−03	2.21E−03	0.0564
$2s^2 2p\ ^2P^\circ_{3/2}$	$2s2p^2\ ^2D_{5/2}$	79.49	79.365	1.56E+10	1.60E+10	8.89E−02	9.11E−02	2.32E−02	2.38E−02	0.0244
$2s^2 2p\ ^2P^\circ_{3/2}$	$2s2p^2\ ^2S_{1/2}$	61.30	61.106	9.20E+10	9.28E+10	1.04E−01	1.04E−01	2.09E−02	2.11E−02	0.0092
$2s^2 2p\ ^2P^\circ_{3/2}$	$2s2p^2\ ^2P_{3/2}$	60.91	60.489	1.35E+11	1.36E+11	3.00E−01	3.03E−01	6.01E−02	6.08E−02	0.0117

Table 4. *Cont.*

Sr										
Transition		**λ (in Å)**	**λ_c (in Å) NIST [44]**	**A**		**gf**		**S**		**dT**
i	**j**			**B**	**C**	**B**	**C**	**B**	**C**	
$2s^2 2p\ ^2P^\circ_{1/2}$	$2s2p^2\ ^4P_{1/2}$	131.09	132.0	1.78E+09	1.92E+09	9.18E−03	9.88E−03	3.96E−03	4.26E−03	0.0704
$2s^2 2p\ ^2P^\circ_{1/2}$	$2s2p^2\ ^4P_{3/2}$	84.49	84.9	8.37E+07	8.77E+07	3.58E−04	3.76E−04	1.00E−04	1.04E−04	0.0460
$2s^2 2p\ ^2P^\circ_{1/2}$	$2s2p^2\ ^2D_{3/2}$	61.41	61.2	6.41E+10	6.55E+10	1.45E−01	1.48E−01	2.93E−02	2.99E−02	0.0214
$2s^2 2p\ ^2P^\circ_{1/2}$	$2s2p^2\ ^2P_{1/2}$	59.11	58.8	1.21E+11	1.23E+11	1.26E-01	1.29E-01	2.46E-02	2.51E-02	0.0180
$2s^2 2p\ ^2P^\circ_{1/2}$	$2s2p^2\ ^2P_{3/2}$	42.28	42.1	8.97E+09	9.00E+09	9.62E-03	9.65E-03	1.34E-03	1.34E-03	0.0037
$2s^2 2p\ ^2P^\circ_{1/2}$	$2s2p^2\ ^2S_{1/2}$	42.47	42.4	6.56E+08	6.70E+08	3.54E-04	3.63E-04	4.96E-05	5.07E-05	0.0222
$2s^2 2p\ ^2P^\circ_{3/2}$	$2s2p^2\ ^4P_{1/2}$	717.22	732.0	1.72E+06	2.26E+06	2.65E-04	3.48E-04	6.26E-04	8.22E-04	0.2376
$2s^2 2p\ ^2P^\circ_{3/2}$	$2s2p^2\ ^4P_{3/2}$	178.52	180.0	8.30E+07	9.51E+07	1.59E-03	1.82E-03	9.32E-04	1.07E-03	0.1272
$2s^2 2p\ ^2P^\circ_{3/2}$	$2s2p^2\ ^4P_{5/2}$	139.42	140.0	1.23E+09	1.36E+09	2.16E-02	2.37E-02	9.90E-03	1.09E-02	0.0913
$2s^2 2p\ ^2P^\circ_{3/2}$	$2s2p^2\ ^2D_{3/2}$	99.51	99.0	1.09E+09	1.16E+09	6.48E−03	6.87E−03	2.12E−03	2.25E−03	0.0563
$2s^2 2p\ ^2P^\circ_{3/2}$	$2s2p^2\ ^2P_{1/2}$	93.60	92.8	2.68E+09	2.86E+09	7.04E−03	7.50E−03	2.17E−03	2.31E−03	0.0621
$2s^2 2p\ ^2P^\circ_{3/2}$	$2s2p^2\ ^2D_{5/2}$	74.38	74.3	1.74E+10	1.80E+10	8.69E−02	8.97E−02	2.13E−02	2.19E−02	0.0312
$2s^2 2p\ ^2P^\circ_{3/2}$	$2s2p^2\ ^2S_{1/2}$	57.76	57.6	1.02E+11	1.04E+11	1.02E−01	1.04E−01	1.94E−02	1.98E−02	0.0156
$2s^2 2p\ ^2P^\circ_{3/2}$	$2s2p^2\ ^2P_{3/2}$	57.41	57.1	1.51E+11	1.54E+11	2.99E−01	3.04E−01	5.65E−02	5.75E−02	0.0172
Ru										
Transition		**λ(in Å)**		**A**		**gf**		**S**		**dT**
i	**j**			**B**	**C**	**B**	**C**	**B**	**C**	
$2s^2 2p\ ^2P^\circ_{1/2}$	$2s2p^2\ ^4P_{1/2}$	103.83		4.08E+09	4.40E+09	1.32E−02	1.42E−02	4.50E−03	4.86E−03	0.0731
$2s^2 2p\ ^2P^\circ_{1/2}$	$2s2p^2\ ^4P_{3/2}$	53.61		3.78E+08	3.93E+08	6.51E−04	6.77E−04	1.15E−04	1.19E−04	0.0390
$2s^2 2p\ ^2P^\circ_{1/2}$	$2s2p^2\ ^2D_{3/2}$	41.81		1.56E+11	1.60E+11	1.64E−01	1.67E−01	2.26E−02	2.30E−02	0.0197
$2s^2 2p\ ^2P^\circ_{1/2}$	$2s2p^2\ ^2P_{1/2}$	41.22		2.40E+11	2.44E+11	1.22E−01	1.24E−01	1.66E−02	1.68E−02	0.0166
$2s^2 2p\ ^2P^\circ_{1/2}$	$2s2p^2\ ^2P_{3/2}$	27.22		1.11E+10	1.11E+10	4.96E−03	4.95E−03	4.44E−04	4.44E−04	0.0009
$2s^2 2p\ ^2P^\circ_{1/2}$	$2s2p^2\ ^2S_{1/2}$	27.29		4.12E+08	4.25E+08	9.20E−05	9.48E−05	8.26E−06	8.52E−06	0.0302
$2s^2 2p\ ^2P^\circ_{3/2}$	$2s2p^2\ ^4P_{1/2}$	458.21		2.37E+06	2.08E+06	2.99E−04	2.62E−04	4.50E−04	3.95E−04	0.1240
$2s^2 2p\ ^2P^\circ_{3/2}$	$2s2p^2\ ^4P_{3/2}$	146.22		1.66E+08	1.90E+08	2.12E−03	2.43E−03	1.02E−03	1.17E−03	0.1282
$2s^2 2p\ ^2P^\circ_{3/2}$	$2s2p^2\ ^4P_{5/2}$	113.10		2.26E+09	2.50E+09	2.60E−02	2.87E−02	0.97E−02	1.07E−02	0.0945
$2s^2 2p\ ^2P^\circ_{3/2}$	$2s2p^2\ ^2D_{3/2}$	82.61		2.59E+09	2.75E+09	1.06E−02	1.13E−02	2.89E−03	3.06E−03	0.0579
$2s^2 2p\ ^2P^\circ_{3/2}$	$2s2p^2\ ^2P_{1/2}$	80.34		4.65E+09	4.98E+09	9.01E−03	9.64E−03	2.38E−03	2.55E−03	0.0650
$2s^2 2p\ ^2P^\circ_{3/2}$	$2s2p^2\ ^2D_{5/2}$	49.58		3.65E+10	3.73E+10	8.07E−02	8.25E−02	1.32E−02	1.35E−02	0.0225
$2s^2 2p\ ^2P^\circ_{3/2}$	$2s2p^2\ ^2S_{1/2}$	40.27		2.02E+11	2.04E+11	9.85E−02	9.94E−02	1.30E−02	1.32E−02	0.0090
$2s^2 2p\ ^2P^\circ_{3/2}$	$2s2p^2\ ^2P_{3/2}$	40.12		3.17E+11	3.21E+11	3.06E−01	3.10E−01	4.04E−02	4.09E−02	0.0121

Table 4. *Cont.*

Sn										
Transition		**λ (in Å)**	**A**		**gf**		**S**		**dT**
i	**j**		**B**	**C**	**B**	**C**	**B**	**C**	
$2s^2 2p\ ^2P^\circ_{1/2}$	$2s2p^2\ ^4P_{1/2}$	85.33	7.11E+09	7.73E+09	1.55E−02	1.69E−02	4.36E−03	4.74E−03	0.0801
$2s^2 2p\ ^2P^\circ_{1/2}$	$2s2p^2\ ^4P_{3/2}$	34.67	1.44E+09	1.49E+09	1.04E−03	1.07E−03	1.18E−04	1.22E−04	0.0335
$2s^2 2p\ ^2P^\circ_{1/2}$	$2s2p^2\ ^2D_{3/2}$	28.64	3.83E+11	3.90E+11	1.88E−01	1.92E−01	1.77E−02	1.81E−02	0.0184
$2s^2 2p\ ^2P^\circ_{1/2}$	$2s2p^2\ ^2P_{1/2}$	28.54	5.12E+11	5.20E+11	1.25E−01	1.27E−01	1.17E−02	1.19E−02	0.0154
$2s^2 2p\ ^2P^\circ_{1/2}$	$2s2p^2\ ^2P_{3/2}$	17.70	1.46E+10	1.45E+10	2.75E−03	2.73E−03	1.60E−04	1.59E−04	0.0049
$2s^2 2p\ ^2P^\circ_{1/2}$	$2s2p^2\ ^2S_{1/2}$	17.73	2.52E+08	2.65E+08	2.37E−05	2.50E−05	1.39E−06	1.46E−06	0.0492
$2s^2 2p\ ^2P^\circ_{3/2}$	$2s2p^2\ ^4P_{1/2}$	112.07	1.11E+08	1.09E+08	8.36E−04	8.18E−04	3.08E−04	3.02E−04	0.0208
$2s^2 2p\ ^2P^\circ_{3/2}$	$2s2p^2\ ^4P_{3/2}$	121.94	2.80E+08	3.27E+08	2.50E−03	2.91E−03	1.00E−03	1.17E−03	0.1418
$2s^2 2p\ ^2P^\circ_{3/2}$	$2s2p^2\ ^4P_{5/2}$	32.98	8.43E+10	8.61E+10	8.25E−02	8.42E−02	8.96E−03	9.15E−03	0.0209
$2s^2 2p\ ^2P^\circ_{3/2}$	$2s2p^2\ ^2D_{3/2}$	70.07	4.39E+09	4.71E+09	1.29E−02	1.39E−02	2.98E−03	3.20E−03	0.0688
$2s^2 2p\ ^2P^\circ_{3/2}$	$2s2p^2\ ^2P_{1/2}$	69.47	6.87E+09	7.44E+09	9.94E−03	1.08E−02	2.27E−03	2.46E−03	0.0758
$2s^2 2p\ ^2P^\circ_{3/2}$	$2s2p^2\ ^2D_{5/2}$	94.74	3.35E+09	3.76E+09	2.70E-02	3.04E-02	8.43E-03	9.48E-03	0.1112
$2s^2 2p\ ^2P^\circ_{3/2}$	$2s2p^2\ ^2S_{1/2}$	27.97	4.28E+11	4.32E+11	1.00E-01	1.01E-01	9.24E-03	9.33E-03	0.0092
$2s^2 2p\ ^2P^\circ_{3/2}$	$2s2p^2\ ^2P_{3/2}$	27.90	7.04E+11	7.12E+11	3.28E-01	3.33E-01	3.02E-02	3.05E-02	0.0125

Ba										
Transition		**λ (in Å)**	**λ_c (in Å) NIST [44]**	**A**		**gf**		**S**		**dT**
i	**j**			**B**	**C**	**B**	**C**	**B**	**C**	
$2s^2 2p\ ^2P^\circ_{1/2}$	$2s2p^2\ ^4P_{1/2}$	71.79	71.654	1.06E+10	1.17E+10	1.65E−02	1.80E−02	3.89E−03	4.27E−03	0.0878
$2s^2 2p\ ^2P^\circ_{1/2}$	$2s2p^2\ ^4P_{3/2}$	22.81	22.947	4.79E+09	4.93E+09	1.51E−03	1.55E−03	1.14E−04	1.17E−04	0.0296
$2s^2 2p\ ^2P^\circ_{1/2}$	$2s2p^2\ ^2D_{3/2}$	19.79	19.769	9.28E+11	9.44E+11	2.18E−01	2.22E−01	1.42E−02	1.44E−02	0.0175
$2s^2 2p\ ^2P^\circ_{1/2}$	$2s2p^2\ ^2P_{1/2}$	19.80	19.778	1.14E+12	1.15E+12	1.34E−01	1.36E−01	8.73E−03	8.86E−03	0.0143
$2s^2 2p\ ^2P^\circ_{1/2}$	$2s2p^2\ ^2P_{3/2}$	11.72	11.710	1.99E+10	1.97E+10	1.64E−03	1.62E−03	6.31E−05	6.26E−05	0.0086
$2s^2 2p\ ^2P^\circ_{1/2}$	$2s2p^2\ ^2S_{1/2}$	11.73	11.730	1.47E+08	1.62E+08	6.08E−06	6.69E−06	2.35E−07	2.58E−07	0.0909
$2s^2 2p\ ^2P^\circ_{3/2}$	$2s2p^2\ ^4P_{1/2}$	49.97	50.140	8.67E+08	8.67E+08	1.30E−03	1.30E−03	2.13E−04	2.13E−04	0.0001
$2s^2 2p\ ^2P^\circ_{3/2}$	$2s2p^2\ ^4P_{3/2}$	103.03	103.316	4.29E+08	5.09E+08	2.73E−03	3.24E−03	9.26E−04	10.99E−04	0.1582
$2s^2 2p\ ^2P^\circ_{3/2}$	$2s2p^2\ ^4P_{5/2}$	22.17	22.183	2.02E+11	2.07E+11	8.96E−02	9.14E−02	6.54E−03	6.67E−03	0.0198
$2s^2 2p\ ^2P^\circ_{3/2}$	$2s2p^2\ ^2D_{3/2}$	60.31	59.934	6.36E+09	6.93E+09	1.39E−02	1.51E−02	2.75E−03	3.00E−03	0.0822
$2s^2 2p\ ^2P^\circ_{3/2}$	$2s2p^2\ ^2P_{1/2}$	60.40	60.024	9.31E+09	10.19E+09	1.02E−02	1.11E−02	2.02E−03	2.22E−03	0.0868
$2s^2 2p\ ^2P^\circ_{3/2}$	$2s2p^2\ ^2D_{5/2}$	80.92	80.736	4.48E+09	5.16E+09	2.64E−02	3.04E−02	7.04E−03	8.09E−03	0.1307
$2s^2 2p\ ^2P^\circ_{3/2}$	$2s2p^2\ ^2S_{1/2}$	19.48	19.473	9.37E+11	9.46E+11	1.07E−01	1.08E−01	6.84E−03	6.90E−03	0.0094
$2s^2 2p\ ^2P^\circ_{3/2}$	$2s2p^2\ ^2P_{3/2}$	19.45	19.420	1.60E+12	1.63E+12	3.64E−01	3.69E−01	2.33E−02	2.36E−02	0.0128

4. Conclusions

In this work, we have provided a detailed and systematic study of fine-structure energy levels, wavelengths, transition rates, and line strengths for transitions among levels belonging to $2s^2 2p$ and $2s2p^2$ configurations of Ge XXVIII, Rb XXXIII, Sr XXXIV, Ru XL, Sn XLVI, and Ba LII. The MCDHF method has been adopted for the calculations. The calculations were performed for valence–valence and core–valence correlations through large configuration expansions in a systematic way using active set approach. The self-consistent field approximation, Breit interaction, and QED effects are included to improve the atomic state functions and the corresponding energies. Results from our present calculations are in good agreement with other available theoretical and experimental results. Nearly equal values of length and velocity forms indicate the accuracy of our results. It is clear that the relativistic and configuration interaction effects are important in the accurate evaluation of atomic data. It is clear that for all Z ions, the MCDHF method including core–valence correlation is an accurate approach for the whole sequence. We hope that these results will be useful for analyzing data from fusion devices and from astrophysical sources and in the modeling and characterization of plasmas.

Acknowledgments: Indu Khatri and Arun Goyal are thankful to U.G.C., India for their Junior Research Fellowship. M.M. Man Mohan is thankful to U.G.C. for Basic Science Research Fellowship.

Author Contributions: Indu Khatri and Arun Goyal proposed the main idea of the paper and performed the calculations. Man Mohan and Avnindra Kumar Singh provided the required computer hardware, were involved in the discussion and in writing the manuscript.

Conflicts of Interest: The authors declare no conflict of interest.

References

1. Landi, E.; Gu, M.F. Atomic data for high-energy configurations in Fe xvii–xxiii. *Astrophys. J.* **2006**, *640*, 1171–1179. [CrossRef]
2. Vilkas, M.J.; Ishikawa, Y.; Träbert, E. Relativistic Many-Body Perturbation Calculations of Boron-Like Silicon, Si X. *Phys. Scr.* **2005**, *72*, 181–199. [CrossRef]
3. Jonauskas, V.; Bogdanovich, P.; Keenan, F.P.; Kisielius, R.; Roord, M.E.; Heeter, R.F.; Rose, S.J.; Ferland, G.J.; Norrington, P.H. Energy levels and transition probabilities for boron-like Fe XXII. *Astron. Astrophys.* **2006**, *455*, 1157–1160. [CrossRef]
4. Wouters, A.; Schwob, J.L.; Suckewer, S.; Seely, J.F.; Feldman, U.; Dave, J.H. Spectra in the 60345-Å wavelength region of the elements Fe, Ni, Zn, Ge, Se, and Mo injected into the Princeton Large Torus tokamak. *J. Opt. Soc. Am. B* **1988**, *5*, 1520–1527. [CrossRef]
5. Myrnäs, R.; Jupen, C.; Miecnik, G.; Martinson, I.; Denne-Hinnov, B. Transitions in boronlike Ni XXIV, Ge XXVIII, Kr XXXII and Mo XXXVIII and fluorinelike Zr XXXII and Mo XXXIV, observed in the JET tokamak. *Phys. Scr.* **1994**, *49*, 429. [CrossRef]
6. Galavís, M.; Mendoza, C.; Zeippen, C. Atomic data from the Iron Project XXIX: Radiative rates for transitions within the n = 2 complex in ions of the boron isoelectronic sequence. *Astron. Astrophys. Suppl. Ser.* **1998**, *131*, 499–522. [CrossRef]
7. Doschek, G.A.; Meekins, J.F.; Cowan, R.D. Spectra of solar flares from 8.5 Å to 16 Å. *Sol. Phys.* **1973**, *29*, 125–141. [CrossRef]
8. Mason, H.E.; Storey, P.J. Atomic data for Fe XII. *Mon. Not. R. Astron. Soc.* **1980**, *191*, 631–639. [CrossRef]
9. Machtoub, G.; López-Urrutia, J.R.C.; Zhang, X.; Tawara, H. Electron–ion interactions for trapped highly charged Ge ions. *Can. J. Phys.* **2006**, *84*, 67–81. [CrossRef]
10. Cheng, K.T.; Kim, Y.K.; Desclaux, J.P. Electric dipole, quadrupole, and magnetic dipole transition probabilities of ions isoelectronic to the first-row atoms, Li through F. *At. Data Nucl. Data Tables* **1979**, *24*, 111–189. [CrossRef]
11. Safronova, U.I.; Johnson, W.R.; Safronova, M.S. Relativistic many-body calculations of energies of n = 3 states for the boron isoelectronic sequence, Z = 6–30. *At. Data Nucl. Data Tables* **1998**, *69*, 183–215. [CrossRef]
12. Zhang, H.L.; Sampson, D.H. Relativistic Distorted-Wave Collision Strengths and Oscillator Strengths for the 105 $\Delta n = 0$ Transitions with n = 2 in the 85 B-Like Ions with $8 \leqslant Z \leqslant 92$. *At. Data Nucl. Data Tables* **1994**, *56*, 41–104. [CrossRef]

13. Vilkas, M.J.; Ishikawa, Y.; Koc, K. Second-order multiconfigurational Dirac–Fock calculations on boronlike ions (pages 813–823). *Int. J. Quant. Chem.* **1998**, *70*, 813–823. [CrossRef]
14. Shirai, T.; Reader, J.; Kramida, A.E.; Sugar, J. Spectral Data for Gallium: Ga I through Ga XXXI. *J. Phys. Chem. Ref. Data* **2007**, *36*, 509–615. [CrossRef]
15. Nahar, S.N. Allowed and forbidden transition parameters for Fe XXII. *At. Data Nucl. Data Tables* **2010**, *96*, 26–51. [CrossRef]
16. Murakami, I.; Safronova, U.I.; Vasilyev, A.A.; Kato, T. Excitation energies, radiative and autoionization rates, dielectronic satellite lines, and dielectronic recombination rates to excited states for B-like oxygen. *At. Data Nucl. Data Tables* **2005**, *90*, 1–74. [CrossRef]
17. Bhatia, A.K.; Feldman, U.; Seely, J.F. Atomic data and spectral line intensities for the boron isoelectronic sequence (Ar XIV through Kr XXXII). *At. Data Nucl. Data Tables* **1986**, *35*, 319–343. [CrossRef]
18. Tachiev, G.; Fischer, C.F. Breit–Pauli energy levels, lifetimes, and transition probabilities for the beryllium-like to neon-like sequences. *At. Data Nucl. Data Tables* **2004**, *87*, 1–184.
19. Tachiev, G.; Fischer, C.F. Breit-Pauli energy levels, lifetimes and transition data: Boron-like spectra. *J. Phys. B At. Mol. Opt. Phys.* **2000**, *33*, 2419–2435. [CrossRef]
20. Fischer, C.F.; Tachiev, G. MCHF/MCDHF Collection, Version 2, Ref. No. 3, 40, National Institute of Standards and Technology. 2011. Available online: http://physics.nist.gov/mchf (accessed on 8 April 2016).
21. Koc, K. Ab initio calculation of $1s^2 2l 3l' 4l''$ energy levels and E1 transition probabilities for O^{3+}. *J. Phys. B At. Mol. Opt. Phys.* **2004**, *37*, 3821–3835. [CrossRef]
22. Koc, K. Relativistic MR RCI Calculation of Energy Levels and Transition Probabilities of Boron Isoelectronic Sequence. *Phys. Scr.* **2003**, *67*, 491–499. [CrossRef]
23. Koc, K. QED effects in transition energies of low lying levels for highly ionized boron like ions. *Nucl. Instr. Meth. Phys. Res. B* **2005**, *235*, 46–50. [CrossRef]
24. Corrégé, G.; Hibbert, A. Transitions in C II, N III, and O IV. *At. Data Nucl. Data Tables* **2004**, *86*, 19–34. [CrossRef]
25. Jönsson, P.; Li, J.; Gaigalas, G.; Dong, C. Hyperfine structures, isotope shifts, and transition rates of C II, N III, and O IV from relativistic configuration interaction calculations. *At. Data Nucl. Data Tables* **2010**, *96*, 271–298. [CrossRef]
26. Li, J.; Jönsson, P.; Dong, C.; Gaigalas, G. Two-electron–one-photon M1 and E2 transitions between the states of the $2p^3$ and $2s^2 2p$ odd configurations for B-like ions with $18 \leqslant Z \leqslant 92$. *J. Phys. B At. Mol. Opt. Phys.* **2010**, *43*, 035005. [CrossRef]
27. Hao, L.; Jiang, G. Energy levels, transition rates, and line strengths of B-like ions. *Phys. Rev. A* **2011**, *83*, 012511. [CrossRef]
28. Rynkun, P.; Jönsson, P.; Gaigalas, G.; Fischer, C.F. Energies and E1, M1, E2, M2 transition rates for states of the 2s22p, 2s2p2, and 2p3 configurations in boron-like ions between N III and Zn XXVI. At. *Data Nucl. Data Tables* **2012**, *98*, 481–556. [CrossRef]
29. Marques, J.P.; Indelicato, P.; Parente, F. Relativistic multiconfiguration calculations of the 2s22p 2P3/2 level lifetime along the boron isoelectronic sequence. *Eur. Phys. J. D* **2012**, *66*, 32. [CrossRef]
30. Zhang, C.M.; Chen, C.; Sun, Y.; Gou, B.C.; Shao, B. Energy, fine structure, hyperfine structure, and radiative transition rates of the high-lying multi-excited states for B-like neon *Eur. Phys. J. D* **2015**, *69*, 105.
31. Chen, C. Energies, expectation values, fine structures and hyperfine structures of the ground state and excited states for boron. *Eur. Phys. J. D* **2015**, *69*, 128. [CrossRef]
32. Reader, J.; Gillaspy, J.D.; Osin, D.; Ralchenko, Y. Extreme ultraviolet spectra and analysis of $\Delta n = 0$ transitions in highly charged barium. *J. Phys. B At. Mol. Opt. Phys.* **2014**, *47*, 145003. [CrossRef]
33. Jönsson, P.; He, X.; Fischer, C.F.; Grant, I.P. The grasp2K relativistic atomic structure package. *Comput. Phys. Commun.* **2007**, *177*, 597–622. [CrossRef]
34. Grant, I.P. *Relativistic Quantum Theory of Atoms and Molecules*; Springer: New York, NY, USA, 2007.
35. McKenzie, B.J.; Grant, I.P.; Norrington, P.H. A program to calculate transverse Breit and QED corrections to energy levels in a multiconfiguration Dirac-Fock environment. *Comput. Phys. Commun.* **1980**, *21*, 233–246. [CrossRef]
36. Gaigalas, G.; Rudzikas, Z.; Fischer, C.F. An efficient approach for spin-angular integrations in atomic structure calculations. *J. Phys. B At. Mol. Opt. Phys.* **1997**, *30*, 3747–3771. [CrossRef]

37. Grant, I.P. Gauge invariance and relativistic radiative transitions. *J. Phys. B. At. Mol. Opt. Phys.* **1974**, *7*, 1458–1475. [CrossRef]
38. Dyall, K.G.; Grant, I.P.; Johnson, C.T.; Parpia, F.A.; Plummer, E.P. GRASP: A general-purpose relativistic atomic structure program. *Comput. Phys. Commun.* **1989**, *55*, 425–456. [CrossRef]
39. Olsen, J.; Roos, B.O.; Jorgensen, P.; Jensen, H.J.A. Determinant based configuration interaction algorithms for complete and restricted configuration interaction spaces. *J. Chem. Phys.* **1988**, *89*, 2185–2192. [CrossRef]
40. Sturesson, L.; Jönsson, P.; Fischer, C.F. JJGEN: A flexible program for generating lists of jj-coupled configuration state functions *Comput. Phys. Commun.* **2007**, *177*, 539–550. [CrossRef]
41. Oslen, J.; Godefroid, M.R.; Jönsson, P.A.; Malmquist, P.A.; Froese, F.C. Transition probability calculations for atoms using nonorthogonal orbitals. *Phys. Rev. E* **1995**, *52*, 4499–4508.
42. Norrington, P.H.; Kingston, A.E.; Boone, A.W. Energy levels and transition probabilities for Fe XXV ions. *J. Phys. B At. Mol. Opt. Phys.* **2000**, *33*, 1767–1788. [CrossRef]
43. Kramida, A.; Ralchenko, Y.; Reader, J.; NIST ASD Team. *NIST Atomic Spectra Database (ver. 5.3)*; National Institute of Standards and Technology: Gaitherburg, MD, USA, 2015; Available online: http://physics.nist.gov/asd (accessed on 23 November 2015).
44. Kramida, A.; Ralchenko, Y.; Reader, J.; NIST ASD Team. *NIST Atomic Spectra Database (ver. 5.2)*; National Institute of Standards and Technology: Gaitherburg, MD, USA, 2014; Available online: http://physics.nist.gov/asd (accessed on 26 August 2015).
45. Farrag, A.; Luc-Koenig, E.; Sinzelle, J. Systematic trends of the relativistic f values for electric dipole transitions within the ground complex of B-like ions. *J. Phys. B At. Mol. Opt. Phys.* **1980**, *13*, 3939–3955. [CrossRef]